Supporting Information

Large-Area Freestanding 2D Ni/Co Vertical Heterostructure with Strong Interfacial Coupling for Efficient Oxygen Evolution Reaction

Manav Saxena [a]*, Sayali Ashok Patil [a], Anjali Prajapati [b], Ranjit Thapa [b], Sebastien Royer [c,d], Pramila K. Misra [e]*

[a] Centre for Nano and Material Sciences, Jain (Deemed-to-be University), Jain Global Campus, Ramanagara, Bangalore 562112, India

[b] Department of Physics, SRM University -AP, Andhra Pradesh 522 240, India

[c] Universit´ e de Lille, CNRS, Centrale Lille, Universit´e Artois, UMR 8181-UCCS-12 Unit´ e de Catalyse et Chimie du Solide, Lille 59000, France

[d]ULCO, EiLCO UCEIV UR 4492 MREI 1, 189 A, Avenue Maurice Schumann 59140

[e]Centre of Studies in Surface Science and Technology, School of Chemistry, Sambalpur University, Jyoti Vihar, Sambalpur 768 019, Odisha, India

Table of Content

1. Experimental section

Materials: Nickel nitrate hexahydrate [($Ni(NO_3)_2.6H_2O$, batch no. C17A/1317/0603/21], Cobalt nitrate hexahydrate [($Co(NO_3)_2.6H_2O$, batch no. G16A/1415/0405/31] and potassium hydroxide [KOH batch no. B173/3210/0805/13] were obtained from SD Fine Chem Limited (India). Hexamethylenetetramine [HMTA, $C_6H_{12}N_4$, batch no. STBG9810] and Ruthenium oxide [RuO_2, batch no. MKCL4231) were purchased from Sigma-Aldrich (India).

Deposition of RuO_2 on Fluorine-doped Tin Oxide (FTO)

To prepare the catalytic ink, 1 mg of commercially available RuO_2 was dispersed in 30 µL of ethanol and 5 µL of a 5 wt% Nafion solution (in aliphatic alcohol) using ultrasonication for 10 min. Subsequently, 10 µL of the resulting ink was drop-cast onto an FTO substrate with an active area of 0.5 cm^2 and dried in a conventional oven at 60 °C for 12 hours.

Material characterization

The surface morphology was examined using field-emission scanning electron microscopy (FESEM, JEOL, Singapore) operated at an accelerating voltage of 10 kV. The nanosheet topography was characterized in non-contact mode with an atomic force microscope (AFM, Park Systems, Germany). Transmission electron microscopy (TEM), high-resolution TEM (HRTEM), and selected area electron diffraction (SAED) analyses were carried out on a JEOL JEM-2100 Plus microscope operated at 200 kV. X-ray photoelectron spectroscopy (XPS) measurements were performed on a Kratos AXIS ULTRA 165 instrument equipped with a monochromatic Al Kα radiation source (E = 1,486.7 eV). The system provides an energy resolution of ~0.40 eV, and high-resolution spectra were acquired at a pass energy of 20 eV. Instrument calibration and analyzer alignment were performed using standard reference materials, and all binding energies were referenced to the C 1s peak of adventitious carbon at 284.8 eV.

Electrochemical Measurement

Electrochemical tests were carried out on an electrochemical workstation (Origalys) using a conventional three-electrode configuration. Prior to electrode preparation, fluorine-doped tin oxide (FTO, 0.5 × 1 cm^2) substrates were cleaned by sequential ultrasonication in acetone, ethanol, and

deionized water for 15 min each. The nanosheet was deposited on the FTO and dried in air at room temperature for 12 h which is act as working electrode, platinum wire and an Ag/AgCl electrode served as the counter and reference electrodes, respectively. All electrodes were immersed in 1 M KOH electrolyte (pH ≈ 14). Prior to measurement, the working electrode was stabilized by soaking in the electrolyte for 10 min, followed by electrochemical activation in the potential window of 0-0.6 V at a scan rate of 10 mV s^{-1}. Potentials recorded against the Ag/AgCl reference were converted to the reversible hydrogen electrode (RHE) scale using: E(RHE) = E (Ag/AgCl) + 0.059*pH + 0.197 V- iR, and overpotential (η) was calculated as: η = E(RHE)-1.236 V. Linear sweep voltammetry (LSV) curves were acquired at 5 mV s^{-1} with iR correction, and current densities were normalized to the electrode's geometric area. Tafel slopes were derived from the polarization curves using the relationship: η = a + blog|j| where η is the overpotential, *a* the Tafel constant, *b* the Tafel slope, and *j* the current density. Electrochemical impedance spectroscopy (EIS) was performed at constant η using a frequency range from 100 kHz to 0.1 Hz with an AC perturbation of 5 mV. The electrochemical double-layer capacitance (C_{dl}) was determined by plotting the capacitive current density [$0.5 \times (j_a - j_c)$] against scan rate, and the slope of this plot was taken as C_{dl}. The electrochemically active surface area (ECSA) was then calculated using: C_{dl} /C_s, where Cs (the specific capacitance of a flat surface under identical conditions) was assumed to be 40 μF cm^{-2}. Cyclic voltammetry (CV) within the non-Faradaic region (0-0.2 V vs Ag/AgCl) at different scan rates was used for this determination. Finally, the surface roughness factor (R_f) was obtained from the ratio of ECSA to the electrode's geometric area.

Computational details:

All the analysis on the model structures are performed by relying on Density Functional Theory (DFT) with help of Vienna Ab initio Simulation Package (VASP) involving spin polarization. To simplify the computational difficulty, the interaction between the frozen core and the outer electrons are simplified as projector augmented wave (PAW).[1] The Perdew-Burke-Ernzerhof (PBE) functional is utilized to describe the Generalized gradient approximation (GGA) scheme[2] and the DFT-D2 method is applied to describe the van der Waals interactions.[3] The Kohn-Sham equations are solved by considering the plane wave cut off energy at 520 eV. To avoid any possible interaction between the lattice and its images, vacuum layer of 15 Å is added along 'z -axis'. The Brillouin zone integrations are carried out by employing Monkhorst–Pack mesh of 5×3×1.

Structural optimizations were done until the total energy converged to 10^{-5} eV per atom and the ionic energy converged to 10^{-3} eV. To enhance the interaction of d electrons in the system, a correction term U = 3.52 eV and 6.20 eV included for cobalt and nickel respectively.

Model Structure: To construct the heterostructures, initially the layered structures are made from the unit cell of $Co(OH)_2$ and $Ni(OH)_2$ which are cleaved along (111) and (100) plane respectively. Next, we have constructed two different bilayer heterostructures, Co/Ni and Ni/Co (Fig. 3d) using the layered structures, where $Co(OH)_2$ and $Ni(OH)_2$ are the respective top layers on the corresponding systems. Both the system consist of total 140 number of atoms and thickness of the both the optimised heterostructures, Co/Ni and Ni/Co are obtained to be 17.24 Å and 15.86 Å respectively.[5] The optimization of model structures done with the help of selective dynamics method (i.e. except the surface atoms, all the atoms were fixed).

Overpotential Calculation: The analysis of OER is performed and the theoretical overpotential values (Table T1) obtained from DFT calculation is with respect to the Reversible Hydrogen Electrode (RHE) scale following the Computational Hydrogen Electrode model (CHE).[4]

A reversible hydrogen electrode is a reference electrode, in which measured potential changes with pH, following the Nernst equation.

Theoretically the equilibrium potential for OER is 1.23 V vs. Standard Hydrogen Electrode (SHE) model (independent of pH). Thus, the equilibrium potential for OER in alkaline medium (pH=14) shifts on the RHE scale as:

$$\mathbf{E_{RHE} = E_{SHE} - (0.0592 \times pH)}$$

E_{RHE} = 1.23 (vs.SHE) - (0.0592×14) ≈ 1.23 V - 0.828 V ≈ 0.40 V

The free energy change of each step in the reaction pathway is defined as,

$$\mathbf{\Delta G = \Delta E_{DFT} + \Delta ZPE - T\Delta S - neU}$$

where, E_{DFT} represents total energy obtained through DFT calculation, ΔZPE is the change in the zero-point energies, ΔS is the change in the entropy, and ne is the no. of electrons transferred, and U is the applied potential. The free energy value for each intermediate step will shift by '−eU' energy. So, each intermediate step in the free energy profile plot is shifted by 0.40 V applied equilibrium potential in alkaline medium and the maximum ΔG value obtained is the overpotential

value. This maximum ΔG occurred for *O → *OOH intermediate step which acts as a potential determining step (PDS).

2. XPS survey spectra of Ni/Co

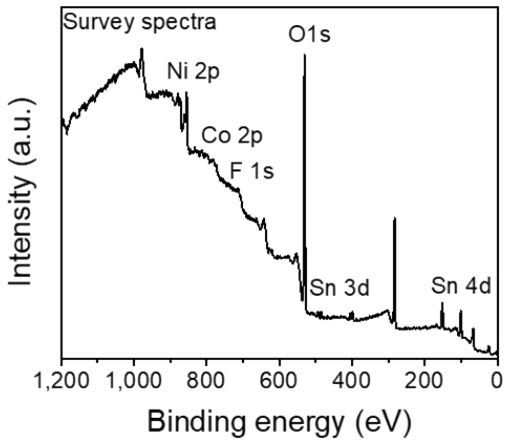

Fig. S1: XPS survey spectra of Ni/Co vertical heterostructure.

3. Charge density difference plots.

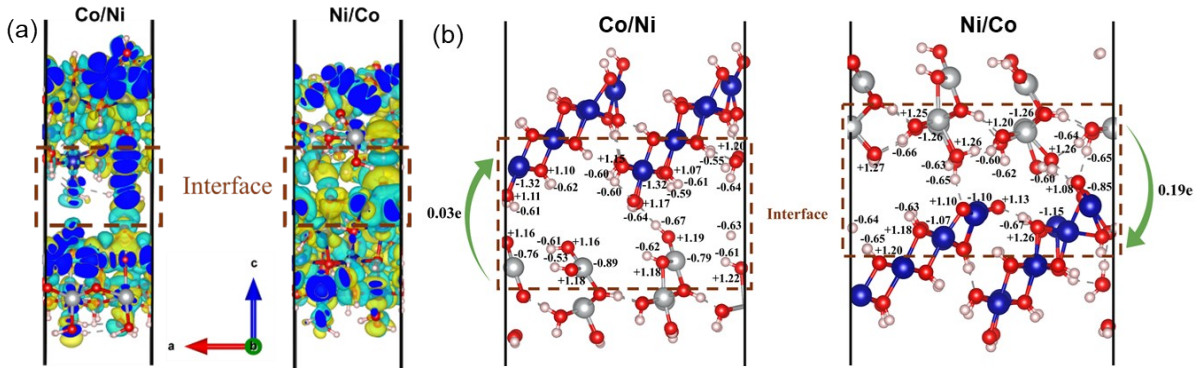

Fig. S2: (a) Charge density difference plots for the Co/Ni and Ni/Co heterostructure respectively where yellow region indicating charge accumulation and cyan region indicating charge depletion. (b) Represents the Bader charge presents on the interfacial atoms and the charge transferred from $Ni(OH)_2$ layer to $Co(OH)_2$ layer for Co/Ni and Ni/Co system respectively.

4. Mass Loading computed by electrochemical method:

Mass loading of catalyst was determined from effective thickness according to procedure reported in previous work.[6]

Mass loading = $(Q \times M)\ /F$

Herein, Q is quantity of electric charge determined by taking integrated area of oxidation peak and represent the in A.s, M represents molecular weight of catalyst in g mol^{-1} (For heterostructure both $Ni(OH)_2$ and $Co(OH)_2$ has been considered), F represents Faraday constant.

Mass loading of Ni/Co = $(Q \times M)\ /F$

= $(0.01679 \times 185.66)/96485 = 32.31\ \mu g$

Mass loading of Co/Ni = $(Q \times M)\ /F$

= $(0.01652 \times 185.66)/96485 = 31.78\ \mu g$

Mass loading of Ni = $(Q \times M)\ /F$

= $(0.0004938 \times 92.70)/\ 96485 = 0.474\ \mu g$

Mass loading of Co = $(Q \times M)\ /F$

= $(0.0006741 \times 92.70)\ /\ 96485 = 0.091\ \mu g$

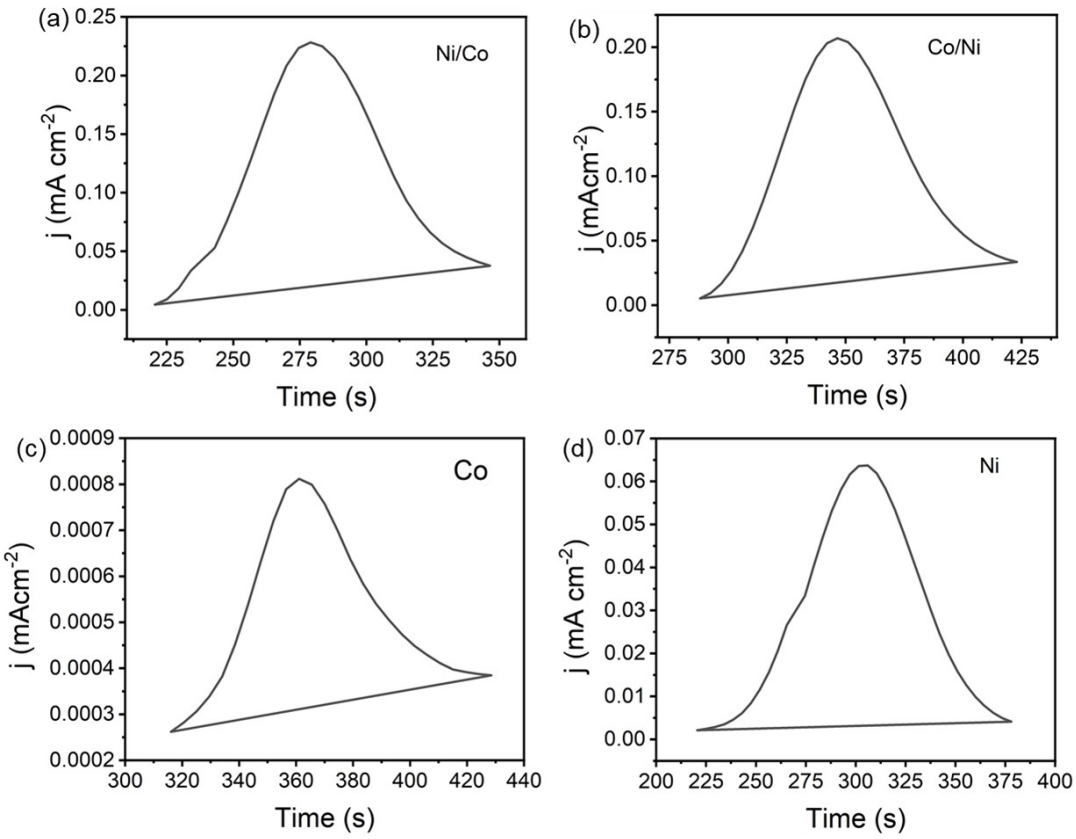

Fig. S3: Area under curves shows of electric charge corresponds to oxidation of (a) Ni/Co, (b) Co/Ni, (c) Ni, (d) Co.

5. CV curve in the non-faradic region and C_{dl} plot of RuO_2.

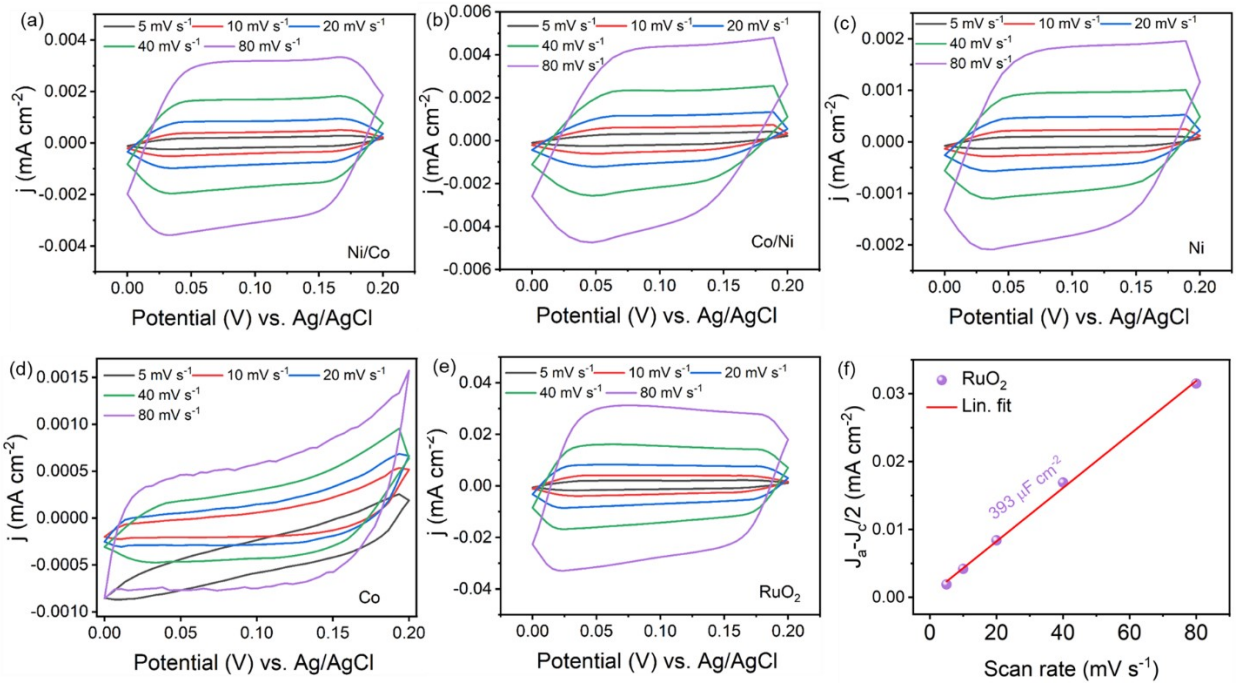

Fig. S4: (a-e) Cyclic voltammograms curves (a) Ni/Co, (b) Co/Ni, (c) Ni, (d) Co, and (e) RuO_2 at different scan rates. (f) C_{dl} plot of RuO_2.

6. Post analysis FESEM image of Ni/Co vertical heterostructure.

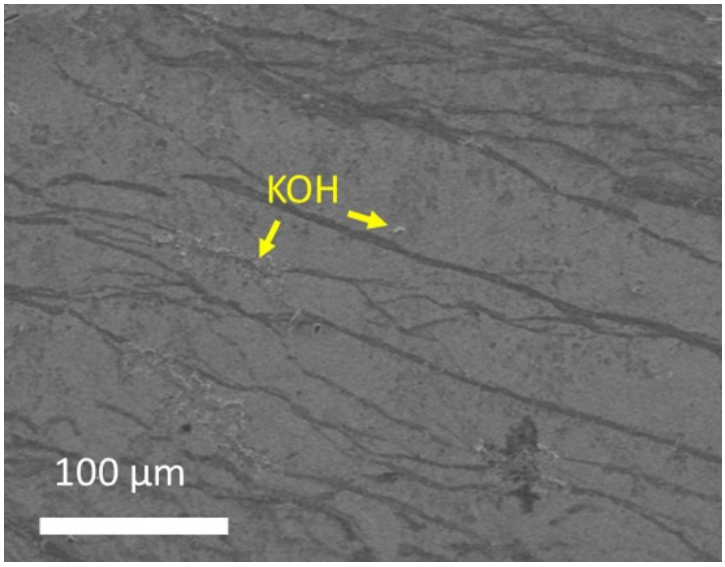

Fig. S5: Post analysis FESEM image of Ni/Co vertical heterostructure.

7. Table T1: Values of the overpotential (η) for respective heterostructures.

Structure	Overpotential (η) vs. RHE
Co/Ni	0.80 V
Ni/Co	0.66 V

8. Table T2: Comparison table of overall OER performances of the optimized heterostructure.

Sl. No.	Catalyst	Onset potential (mV)	Over-potential (mV)	Tafel (mV dec^{-1})	C_{dl} (μF cm^{-2})	ECSA (cm^{-2})	RF
1.	Ni/Co	257	364	70	51	1.28	2.56
2.	Co/Ni	346	417	72	38	0.95	1.9
3.	Ni	389	439	87	22	0.55	1.1
4.	Co	405	475	97	6	0.15	0.3
5.	RuO_2	216	341	63	393	9.83	19.66

9. Table T3: Comparison table of OER performances of the Ni/Co electrocatalysts in alkaline medium.

Sl. No.	Catalyst	Electrolyte	η_{10} (mV)	Tafel (mV dec^{-1})	Stability	Ref.
1.	MWCNT- $Ni(OH)_2$ nanoplate	0.1 M KOH	474	87	6 h	[7]
2.	FeNC/NiO	1 M KOH	390	76	15 h	[8]
3.	$NiCo_2O_4$	1 M NaOH	380	62	-	[9]
4.	Rod-$CoMoO_4$	1 M KOH	384	165	12 h	[10]
5.	$CeO_2/Co(OH)_2$	1 M KOH	410	66	50 h	[11]
6.	$NiCo_2O_4$ Nanoflakes/Ti_4O_7	1 M KOH	398	64	1.11 h	[12]
7.	CoMnNiS	1 M KOH	371	48	-	[13]
8.	**Ni/Co**	**1 M KOH**	**364**	**70**	**13 h**	**This work**

References:

1. P. E. Blöchl, *Physical Review B*, 1994, **50**, 17953-17979.
2. J. P. Perdew, K. Burke and M. Ernzerhof, *Physical Review Letters*, 1996, **77**, 3865-3868.
3. S. Grimme, J. Antony, S. Ehrlich and H. Krieg, *The Journal of Chemical Physics*, 2010, **132**, 154104.
4. J. Rossmeisl, A. Logadottir and J. K. Nørskov, *Chemical Physics*, 2005, **319**, 178-184.
5. S. A. Patil, P. B. Jagdale, N. Barman, A. Sfeir, M. Pathak, S. Royer, R. Thapa, A. K. Samal and M. Saxena, *ChemSusChem*, 2025, **18**, e202500850.
6. P. Tian, Y. Yu, X. Yin and X. Wang, *Nanoscale*, 2018, **10**, 5054-5059.
7. X. Zhou, Z. Xia, Z. Zhang, Y. Ma and Y. Qu, *Journal of Materials Chemistry A*, 2014, **2**, 11799-11806.
8. Z. Zhang, Y. Qin, M. Dou, J. Ji and F. Wang, *Nano Energy*, 2016, **30**, 426-433.
9. C. L. I. Flores, G. Gupta, M. Mamlouk and M. D. L. Balela, *Materials for Renewable and Sustainable Energy*, 2024, **13**, 279-290.
10. K. Prasad, N. Mahato, K. Yoo and J. Kim, *Journal*, 2023, **16**.
11. M.-C. Sung, G.-H. Lee and D.-W. Kim, *Journal of Alloys and Compounds*, 2019, **800**, 450-455.
12. Z. Zheng, W. Geng, Y. Wang, Y. Huang and T. Qi, *International Journal of Hydrogen Energy*, 2017, **42**, 119-124.
13. M. Verma, L. Sinha and P. M. Shirage, *Journal of Materials Science: Materials in Electronics*, 2021, **32**, 12292-12307.